Article

Cell Reports

# A Dual-Sensing Receptor Confers Robust Cellular Homeostasis

## Graphical Abstract

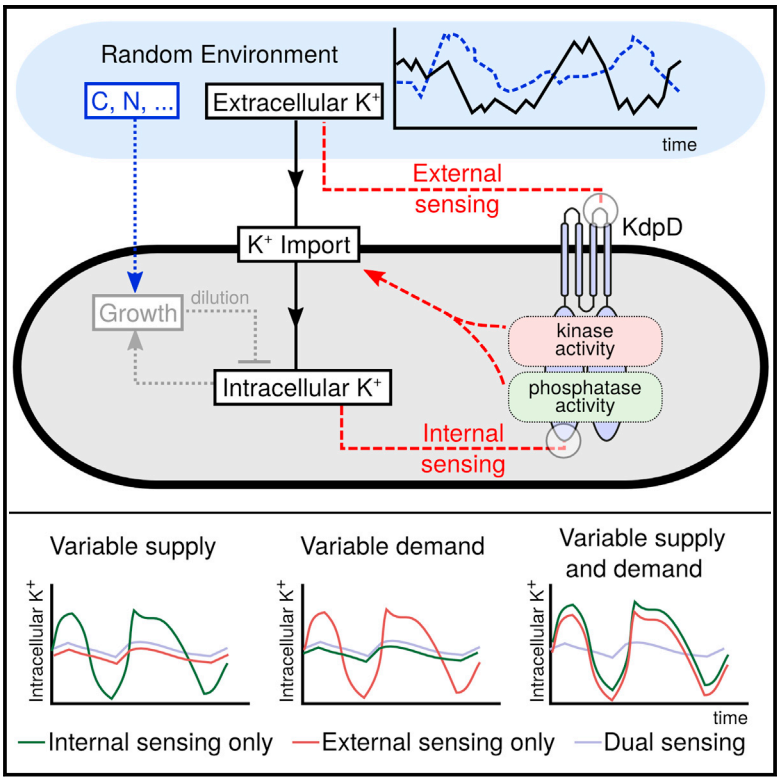


## Highlights

- The bifunctional receptor KdpD senses extra- and intracellular $K^+$
- Kinase and phosphatase activities are regulated by $K^+$
- The dual-sensing strategy is superior under fluctuating conditions

## Authors

Hannah Schramke, Filipe Tostevin, Ralf Heermann, Ulrich Gerland, Kirsten Jung

## Correspondence

gerland@tum.de (U.G.), jung@lmu.de (K.J.)

## In Brief

Schramke et al. find that the bifunctional receptor KdpD regulates its kinase and phosphatase activities by sensing extra- and intracellular $K^+$. Under fluctuating conditions, this dual-sensing strategy ensures robust homeostasis and outcompetes simpler strategies.

Schramke et al., 2016, Cell Reports *16*, 213–221
June 28, 2016 
http://dx.doi.org/10.1016/j.celrep.2016.05.081

Cell Reports
Article



# A Dual-Sensing Receptor Confers Robust Cellular Homeostasis

Hannah Schramke,[1,2,4] Filipe Tostevin,[3,4] Ralf Heermann,[2] Ulrich Gerland,[3,*] and Kirsten Jung[1,2,*]
[1]Center for Integrated Protein Science Munich (CiPSM)
[2]Department of Biology I, Microbiology
Ludwig-Maximilians-Universität München, Großhaderner Straße 2-4, 82152 Martinsried, Germany
[3]Physik Department, Technische Universität München, James Franck Straße 1, 85747 Garching, Germany
[4]Co-first author
*Correspondence: gerland@tum.de (U.G.), jung@lmu.de (K.J.)
http://dx.doi.org/10.1016/j.celrep.2016.05.081

## SUMMARY

**Cells have evolved diverse mechanisms that maintain intracellular homeostasis in fluctuating environments. In bacteria, control is often exerted by bifunctional receptors acting as both kinase and phosphatase to regulate gene expression, a design known to provide robustness against noise. Yet how such antagonistic enzymatic activities are balanced as a function of environmental change remains poorly understood. We find that the bifunctional receptor that regulates $K^+$ uptake in *Escherichia coli* is a dual sensor, which modulates its autokinase and phosphatase activities in response to both extracellular and intracellular $K^+$ concentration. Using mathematical modeling, we show that dual sensing is a superior strategy for ensuring homeostasis when both the supply of and demand for a limiting resource fluctuate. By engineering standards, this molecular control system displays a strikingly high degree of functional integration, providing a reference for the vast numbers of receptors for which the sensing strategy remains elusive.**

## INTRODUCTION

While bacteria have a limited ability to manipulate their environment, they have a remarkable capacity to adapt to changing environmental conditions while maintaining intracellular homeostasis. Two-component signaling, encompassing sensing and regulatory responses, is a major adaptation mechanism in prokaryotes. Like many control systems designed by engineers, the molecular control systems used by cells must operate under unpredictable conditions. To understand the designs that evolved in bacteria long before engineering principles were developed, we are studying the KdpD/KdpE system as a model system, one of the most widespread two-component systems in bacteria and archaea (Heermann and Jung, 2012). This system regulates $K^+$ homeostasis by controlling the production of the high-affinity $K^+$ transporter KdpFABC (Altendorf et al., 1992; Buurman et al., 2004). $K^+$ is the most abundant cation in all living cells, and it is crucial for the regulation of turgor and pH, as well as for the activation of several enzymes (Booth, 1985; Epstein, 2003; Nissen et al., 2000). Even though [$K^+$] is low in many environments, bacteria manage to maintain high intracellular $K^+$ concentrations. As illustrated in Figure 1A, the external availability of $K^+$ is expected to vary wildly, while the dilution of internal $K^+$ by cell growth depends on other fluctuating variables like carbon and nitrogen availability. When $K^+$ is abundant, the constitutive low-affinity $K^+$ transport systems Trk and Kup provide *Escherichia coli* cells with sufficient $K^+$, while KdpFABC can supply additional influx under $K^+$ limitation (Altendorf et al., 1992). How can a two-component system ensure optimal control of these operations under a wide variety of external and internal conditions?

The molecular architecture of the control system is illustrated in Figure 1B. The membrane-integrated receptor (sensor kinase) KdpD senses $K^+$ limitation, autophosphorylates, and transfers the phosphoryl group to the cytoplasmic transcriptional (response) regulator KdpE, resulting in *kdpFABC* expression. KdpD also exhibits phosphatase activity toward phospho-KdpE, which switches the signaling cascade off (Jung et al., 1997). Bifunctional enzymes acting as both autokinase and phosphatase are found in many two-component systems, and they were shown to render the response less sensitive to fluctuations in the concentrations of the two components (Batchelor and Goulian, 2003) or other factors such as ATP availability (Shinar et al., 2007). However, how the cell regulates the two enzymatic activities as a function of the sensed stimuli remains obscure.

KdpD activity is known to be modulated by $K^+$, since in vitro reconstruction of the KdpD/KdpE signaling cascade from purified components revealed an inhibitory effect of $K^+$ on KdpD-mediated phosphorylation of KdpE (Heermann et al., 2009; Lüttmann et al., 2009). However, no binding site for $K^+$ has ever been detected, and it is still unclear whether KdpD senses the extra- or intracellular $K^+$ concentration (Heermann et al., 2014; Laermann et al., 2013). Here we show that both enzymatic activities of the bifunctional receptor KdpD are directly influenced by $K^+$. Recognition of extracellular, periplasmic $K^+$ and intracellular, cytoplasmic $K^+$ results in the inhibition of autokinase activity and the stimulation of phosphatase activity, respectively. Mathematical modeling reveals that this dual-sensing and

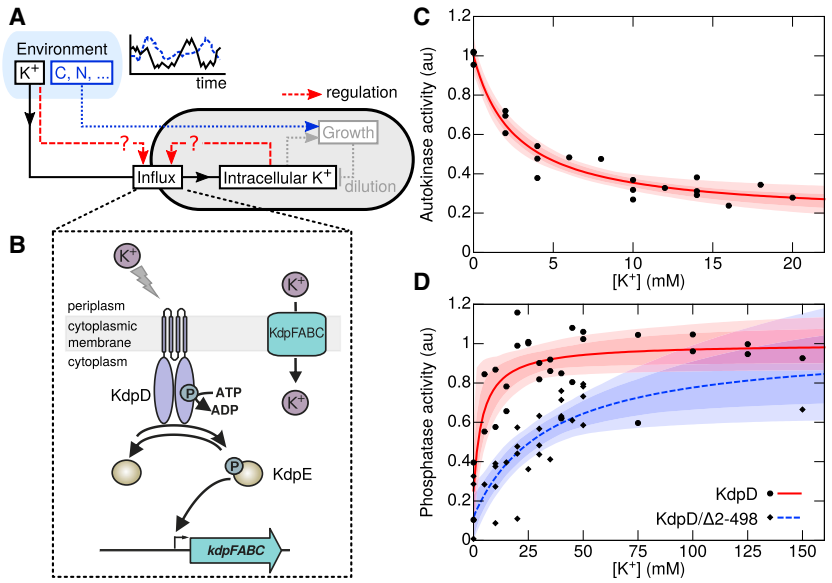


**Figure 1. Sensing of $K^+$ by the Bifunctional Receptor KdpD**

(A) Bacteria in varying environments must regulate their uptake of a limiting resource (here $K^+$). Uptake can be regulated in accordance with the availability of or the bacteria's need for the resource or a combination of both. Other environmental factors may non-specifically affect the demand for the resource, for example, by altering the growth rate.

(B) Schematic of the Kdp regulation system. The bifunctional receptor KdpD acts as both an autokinase (including phosphotransferase) and phosphatase for the response regulator KdpE. Phosphorylated KdpE activates expression of the genes encoding the high-affinity $K^+$ transporter KdpFABC.

(C and D) KdpD autokinase activity (C) and phosphatase activity (D) both depend on $K^+$ concentration. Autokinase activity was determined from the initial rates of KdpD autophosphorylation; phosphatase activity was determined from the initial rate of KdpE-P dephosphorylation by wild-type KdpD or by KdpD/Δ2–498. Lines show the best-fit Michaelis form; shading denotes regions that contain all activity curves within 68% and 95% confidence limits.

regulation strategy is superior for homeostasis when both the environmental supply and the demand for $K^+$ vary.

## RESULTS

### Extracellular $K^+$ Inhibits the Autokinase Activity and Intracellular $K^+$ Stimulates the Phosphatase Activity of KdpD

To analyze how $K^+$ affects signal transduction from KdpD to KdpE, we sought to understand how $K^+$ influenced the rates of each of the two enzymatic activities of KdpD (namely autokinase and phosphatase activities). It should be noted that phosphorylated KdpD immediately transfers the phosphoryl group to KdpE (phosphotransferase activity) (Jung et al., 1997). We first tested the influence of $K^+$ on the autokinase activity of KdpD in vitro by examining the phosphorylation of KdpD in the absence of KdpE. For these experiments, we used membrane vesicles prepared from disrupted cells. A large proportion of the vesicles produced in this way is ruptured or otherwise not sealed off, such that both the cytoplasmic and periplasmic portions of KdpD are accessible to $K^+$ (Mével-Ninio and Yamamoto, 1974; Zeng et al., 1998). The quantitative dependence of the autophosphorylation rate on the $K^+$ concentration is plotted in Figure 1C, showing that $K^+$ inhibits this enzymatic activity with half-maximal inhibition at $K_{0.5} = 2.7^{+1.1}_{-0.7}$ mM (upper and lower bounds of 68% confidence range).

We next studied the dependence of the KdpD phosphatase activity on $K^+$ by measuring the rate of dephosphorylation of phospho-KdpE in vitro in the absence of KdpD autophosphorylation. The quantitative dependence of the dephosphorylation rate on $K^+$ concentration is plotted in Figure 1D, and it shows half-maximal activation at $K_{0.5} = 4.2^{+7.8}_{-3.0}$ mM. $K^+$ therefore has both an inhibitory effect on the autokinase activity and a stimulating effect on the phosphatase activity of KdpD.

The cytoplasmic C-terminal domain of the 894-amino-acid-long KdpD, KdpD/Δ2–498 (Figure 2A), has been proposed to harbor a $K^+$ sensor (Rothenbücher et al., 2006). Having found that purified KdpD/Δ2–498 showed $K^+$-independent autokinase activity (Figure 2B), we hypothesized that this variant might have a $K^+$-dependent phosphatase activity. We therefore tested the effect of $K^+$ on the phosphatase activity of KdpD/Δ2–498 using phospho-KdpE as substrate. The quantitative dependence of the dephosphorylation rate on $K^+$ concentration is plotted in Figure 1D, showing a stimulatory effect with half-maximal activity at $K_{0.5} = 34^{+52}_{-19}$ mM $K^+$. This demonstrated that the C-terminal domain is sufficient for regulation of the phosphatase activity, but not the autokinase activity.

To search for a domain bearing a $K^+$ recognition site, we tested the $K^+$-dependent autokinase activity of several truncated KdpD proteins. The input domain of KdpD consists of the conserved KdpD domain, the Usp domain, four transmembrane helices, and the GAF domain (Heermann and Jung, 2012) (Figure 2A). Remarkably, the autokinase activity of a truncated KdpD variant that lacked the Kdp and Usp domains but still retained the four transmembrane helices (KdpD/Δ12–395, Figure 2) displayed a $K^+$ sensitivity similar to that of wild-type KdpD. Therefore, we focused on a stretch of conserved amino acids in the second periplasmic loop (loop 3) (Figure 3A), and we employed a systematic alanine mutagenesis screen. Using an *E. coli* $P_{kdpFABC}$::*lacZ* reporter strain, we found that KdpD variants with alanine substitutions at amino acid positions Pro466, Thr469, Leu470, and Val472 were less $K^+$ sensitive and that these mutations shifted the onset of *kdpFABC* expression to external $K^+$ concentrations that would normally inhibit expression (Figure 3B).

Finally, we generated a KdpD variant in which all four of these amino acids were replaced with alanine and designated this variant as $KdpD^1$ (Figure 4A). $KdpD^1$ was characterized by a $K^+$-independent autokinase activity and a $K^+$-sensitive phosphatase activity for KdpE-P in vitro (Figure 4B). The regulation of the phosphatase activity was found to be similar to the C-terminal KdpD/Δ2–498 fragment ($K_{0.5} = 32^{+71}_{-18}$ mM $K^+$; Figure S1). Further evidence for $K^+$ recognition by the second periplasmic loop was

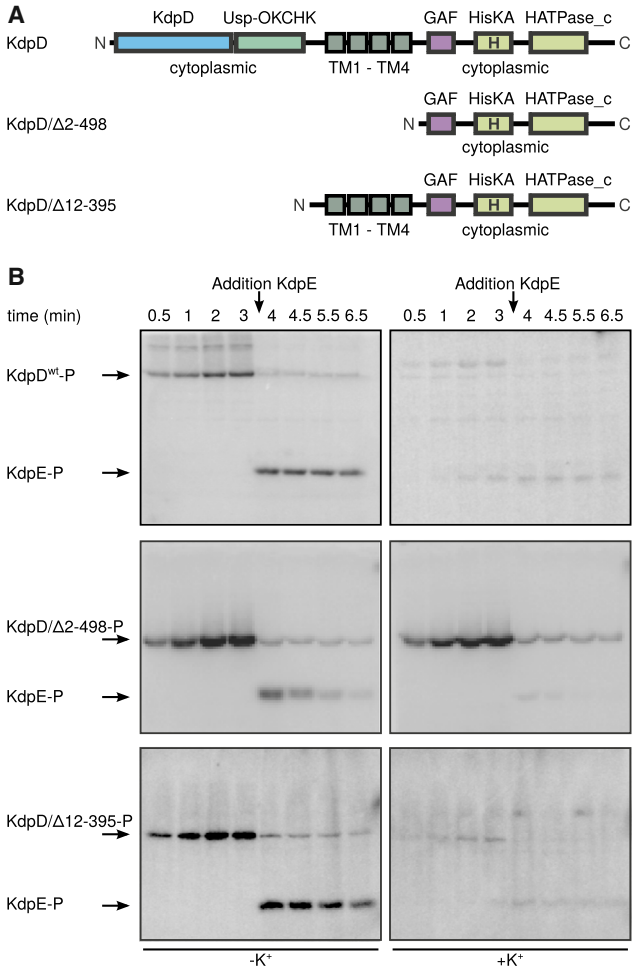


**Figure 2. In Vitro Activities of Truncated KdpD Variants**

(A) Schematics show wild-type KdpD in comparison to the truncated variants KdpD/Δ2–498 and KdpD/Δ12–395. TM, transmembrane helix.

(B) Time-dependent autophosphorylation of KdpD and truncated KdpD variants and dephosphorylation of KdpE in the absence (–) and presence (+) of 250 mM $K^+$ at constant ionic strength. Shown are representative autoradiographs of three independent experiments.

provided by variants in which the N- and C-terminal cytoplasmic domains of KdpD were connected by different linkers. When the two domains were connected by a 5Gly/5Ala or a 10Gly linker, *kdpFABC* expression in the reporter strain was no longer repressed at high [$K^+$]; however, when the domains were linked by the periplasmic loop sequence, repression at high [$K^+$] was restored (Figure S2). Together, these data suggest that the second periplasmic loop of KdpD contains a specific $K^+$ recognition site that regulates autokinase activity in response to extracellular $K^+$.

We next turned to the $K^+$-dependent regulation of the phosphatase activity. As mentioned above, the C-terminal cytoplasmic domain of KdpD has a $K^+$-dependent phosphatase activity (Figure 1D). However, in spite of intensive efforts, we could not localize a $K^+$ recognition site in this domain. In an attempt to circumvent this difficulty, we asked whether loss of the phosphatase activity affected the $K^+$ dependence of the autokinase activity. Amino acid substitutions at position Thr677 in KdpD are known to eliminate the phosphatase activity (Figure 4A) (Brandon et al., 2000), as do substitutions of the same conserved threonine residue in many other sensor kinases (Willett and Kirby, 2012). We therefore assayed the activity of the KdpD variant Thr677→Ala ($KdpD^2$) in vitro. The data revealed that, although $KdpD^2$ lacked phosphatase activity, it retained $K^+$-sensitive autokinase activity (Figure 4B). Thus, how exactly $K^+$ modulates the phosphatase activity of KdpD remains unclear; it may act via the cytoplasmic GAF domain (residues 515–655), since GAF domains are well-known ligand-binding sites also for ions (Cann, 2007a, 2007b; Heikaus et al., 2009). However, our data clearly demonstrate that the autokinase and phosphatase activities of KdpD are individually regulated by $K^+$.

Next we combined the mutations of *kdpD*$^1$ and *kdpD*$^2$, and we found that the resulting $KdpD^{1+2}$ variant had an additive phenotype, displaying a $K^+$-independent autokinase activity and no phosphatase activity such that KdpE remained stably phosphorylated (Figure 4B). Taken together, these results support the idea that KdpD senses extracellular $K^+$ via the periplasmic loop to control its autokinase activity, while intracellular $K^+$ boosts its phosphatase activity.

## Regulation of Both Enzymatic Activities Is Essential for a Controlled Stress Response

To probe the functional behavior of the Kdp system in vivo, we shifted exponentially growing *E. coli* MG1655 cells from $K^+$-saturating conditions to media that imposed different degrees of $K^+$ limitation, and we monitored extra- and intracellular $K^+$ levels and growth over time (Figure 5B; Figure S3). The cells maintained $K^+$ homeostasis until extracellular $K^+$ was completely exhausted, but they continued to grow beyond this point, thus progressively diluting their intracellular pool of $K^+$. The decrease in intracellular [$K^+$] was in turn accompanied by a gradual reduction in the growth rate of the population. We then probed the response mediated by wild-type KdpD as well as that of variants $KdpD^1$, $KdpD^2$, and $KdpD^{1+2}$ by quantifying the production of the high-affinity transporter KdpFABC 2 hr after shifting cells to media with different $K^+$ concentrations covering a broad range of $K^+$ availability (Figure 5C). Wild-type KdpD mediated a graded KdpFABC response at external $K^+$ concentrations below 5 mM. The $KdpD^1$ variant displayed this behavior only at very low $K^+$ concentrations, such that KdpFABC was produced at a constant rate at [$K^+$] > 1 mM, which was consistent with its $K^+$-independent autokinase activity. The $KdpD^2$ variant was less sensitive to intracellular $K^+$ than the wild-type, highlighting the importance of the counteracting phosphatase activity in ensuring a tightly controlled stress response. Finally, in cells harboring the $KdpD^{1+2}$ variant, KdpFABC production became essentially independent of [$K^+$]. Similar results were obtained on the basis of $P_{kdpFABC}$::*lacZ* promoter activity (Figure 3C).

## A Mathematical Model Describes the In Vivo Response Dynamics

To quantitatively explore the consequences of different regulatory strategies, we developed a mathematical model for the relevant aspects of the Kdp system, including the dynamics of

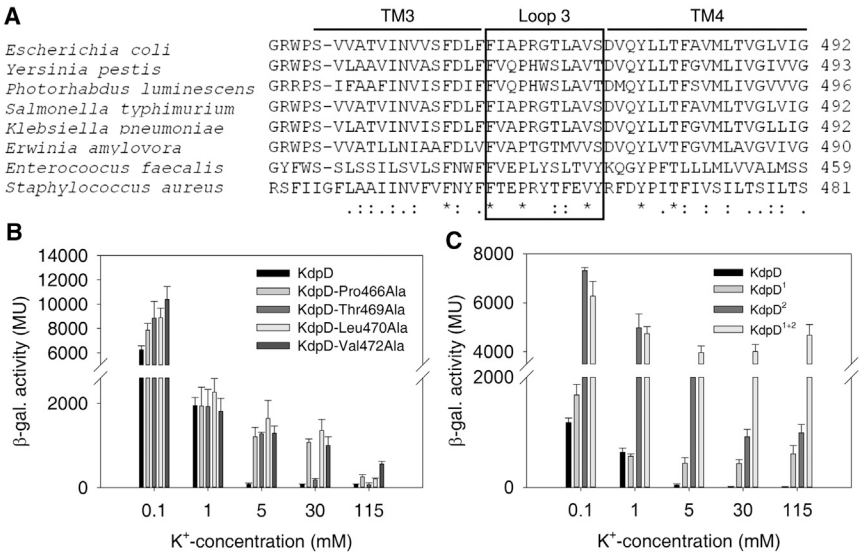


**Figure 3. The Periplasmic Loop between Transmembrane Helix Three and Four Is Involved in $K^+$ Sensing**

(A) Multiple sequence alignment of the periplasmic loop (loop 3) between transmembrane helix 3 (TM3) and helix 4 (TM4). The alignment was created using the ClustalW2 program (Goujon et al., 2010). Protein sequences were as follows: *E. coli*, UniProt: P21865; *Y. pestis*, UniProt: Q7CJR5; *P. luminescens*, UniProt: B6VN55; *S. typhimurium*, UniProt: A0A0D6H090; *K. pneumoniae*, UniProt: B5XZF1; *E. amylovora*, UniProt: D4I3U7; *E. faecalis*, UniProt: Q838F4; and *S. aureus*, UniProt: A0A0H2XIE2.

(B) The β-galactosidase activities of the reporter strain ($P_{kdpFABC}$::*lacZ*) carrying plasmids encoding KdpD and the variants KdpD-Pro466Ala, KdpD-Thr469Ala, KdpD-Leu470Ala, and KdpD-Val472Ala were determined after cultivation of cells in minimal medium at the indicated $K^+$ concentrations.

(C) The β-galactosidase activities of the reporter strains LF3, HS2, HS3, and HS4 ($P_{kdpFABC}$::*lacZ*) carrying KdpD and the variants $KdpD^1$, $KdpD^2$, and $KdpD^{1+2}$ were determined after cultivation of cells in minimal medium at the indicated $K^+$ concentrations.

KdpD/KdpE phosphorylation, rates of KdpFABC production and turnover, rates of $K^+$ import by both KdpFABC and constitutive transporters, and $K^+$-dependent growth (see the Supplemental Experimental Procedures for details). While previous models were forced to make ad hoc assumptions about the regulation of the Kdp response (Heermann et al., 2014), we used the enzymatic activities measured in vitro (Figures 1C and 1D) to parameterize the effects of both extracellular and intracellular $K^+$ on KdpD.

Structural data for bifunctional sensor kinases have suggested the existence of distinct conformational states that possess either autokinase or phosphatase activity (Marina et al., 2005; Ferris et al., 2012; Huynh and Stewart, 2011). Our observation that $KdpD^1$ possesses $K^+$-independent autokinase activity but retains $K^+$-sensitive phosphatase activity is inconsistent with a simple two-state model in which KdpD is always either autokinase or phosphatase active, which implies that the two activities must always be anti-correlated. We therefore considered an extension of this model consisting of three distinct conformational states of KdpD, corresponding to autokinase-active, phosphatase-active, and inactive conformations (Figure 5A). Switching among these states was assumed to obey thermodynamic equilibrium statistics (Bhate et al., 2015), with switching constants that vary depending on the extra- and intracellular concentrations of $K^+$. In such a model, the autokinase and phosphatase activities are correlated and both depend on extra- and intracellular $K^+$. The parameters of these switching constants were determined by fitting to the in vitro enzymatic activities of wild-type KdpD and the $KdpD^1$ variant (Figures 1C and 1D; Figure S1), assuming that the observed activity is proportional to the fraction of KdpD molecules in the corresponding conformational state.

The resulting parameterized switching model was then used as the input into a coarse-grained description of KdpD/KdpE signaling and response via *kdpFABC* expression. Parameters for this larger model were taken from the literature where possible or otherwise fit to experimental data. The model was able to reproduce both the phosphorylation dynamics in vitro (Figure S4) and the in vivo response (Figures 5B and 5C, lines) for wild-type KdpD and the variants $KdpD^1$, $KdpD^2$, and $KdpD^{1+2}$, showing that our regulation model is able to capture the main features of KdpD/KdpE signal transduction.

## Dual Sensing by a Bifunctional Receptor Ensures Robust Homeostasis in Fluctuating Environments

We next sought to compare the performance of cells employing the dual-sensing strategy to that of mutants with only internal or external sensing under conditions of unpredictable environments (illustrated in Figure 1A). The strains carrying *kdpD*$^1$ and *kdpD*$^2$ mutations were unsuited for this purpose, since these cells constitutively produce high levels of the $K^+$ transporter. We therefore employed our model to compare the following three alternative regulation strategies (Figure 6A): (1) the DUAL strategy of wild-type KdpD featuring dual-sensing and bifunctional activities, as revealed by our experiments; (2) external sensing (EX) only, where the enzymatic activities of KdpD are dependent on extracellular $K^+$ but are insensitive to changes in intracellular $K^+$; and (3) internal sensing (IN) only, where the enzymatic activities of KdpD are responsive to intracellular, but not extracellular, $K^+$.

We first asked how accurately each strategy was able to regulate the $K^+$ uptake flux in response to varying $K^+$ supply by comparing steady-state intracellular $K^+$ levels across a range of extracellular $K^+$ concentrations (Figure S5A). The DUAL strategy showed less variability than the IN strategy, which can trigger $K^+$ uptake only after intracellular $[K^+]$ has changed. However, the differences between the DUAL and EX strategies were small, indicating that the additional feedback from intracellular $K^+$ to uptake plays little role under constant conditions.

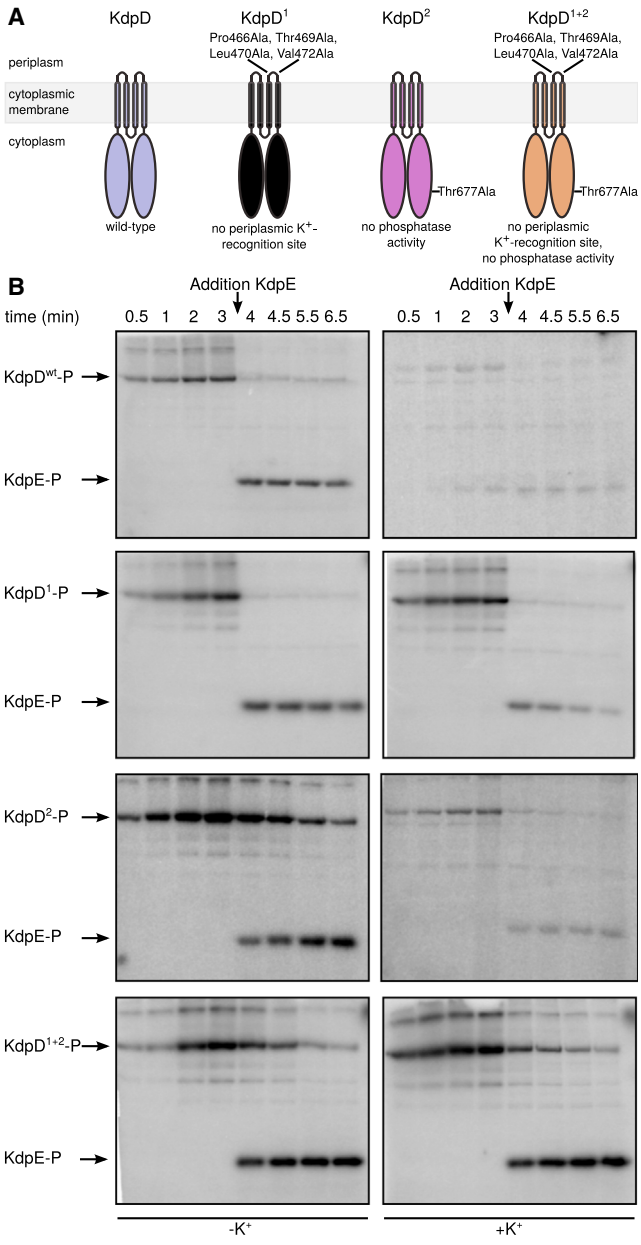


**Figure 4. KdpD Senses Extracellular and Intracellular $K^+$**

(A) Topology model of wild-type KdpD and the locations of amino acid substitutions. Variant $KdpD^1$ contains four amino acid substitutions (Pro466→Ala, Thr469→Ala, Leu470→Ala, and Val472→Ala) in the periplasmic loop region. $KdpD^2$ contains a single substitution (Thr677→Ala) in the C-terminal domain. $KdpD^{1+2}$ combines these five substitutions.

(B) Time-dependent autokinase activity of KdpD and KdpD variants in membrane vesicles was monitored by incubation with [$\gamma$-$^{32}$P]ATP in the presence and absence of $K^+$. After 3.5 min, KdpE was added and phosphotransfer and time-dependent dephosphorylation were monitored. Phosphorylated KdpD and KdpE were separated by SDS-PAGE and gels were exposed to a phosphoscreen. Due to the use of membrane vesicles, a number of unspecific bands are detectable, as, for example, seen in the top right picture, in which KdpD autokinase activity is completely inhibited by $K^+$. See Figure S6 for plots of the phosphorylation time courses, as obtained by quantification of the band intensities.

We reasoned that internal sensing could be beneficial if the intracellular $K^+$ level were to change independently of the extracellular environment. Crucially, the intracellular $K^+$ concentration depends on both the uptake rate and the rate of dilution due to growth (Figure 6B). If cells were exposed to environmental fluctuations that affected growth in a $K^+$-independent manner (e.g., changing carbon or nitrogen availability), the intracellular $K^+$ concentration would be altered even though the environmental $K^+$ level was unchanged. We therefore simulated direct competition among the strategies, which differ only in the regulation of KdpD activity as a function of $K^+$ level, under conditions of fluctuating $K^+$ supply and fluctuations in the maximal growth rate (Figure 6B). In our model the instantaneous growth rate is taken to be a monotonic, saturating function of the intracellular $K^+$ concentration, with a prefactor determined by the environment; thus, differences in the growth rate among strategies reflect differences in intracellular $K^+$ depletion. We found that both the EX and IN strategies were outcompeted by the DUAL strategy, which ultimately came to dominate the population (Figure 6C). The poor performance of the EX strategy in this competition was primarily due to its inability to respond to the increasing demand for $K^+$ under conditions of rapid growth. This dominance of dual sensing over internal sensing is due to its ability to achieve $K^+$ homeostasis more reliably (Figure S6B), as also was observed in the constant environments. The advantage of the DUAL strategy may in fact be greater than estimated here, as our model does not include any penalty for the superfluous overproduction of KdpFABC in high [$K^+$] environments.

## DISCUSSION

Conservation of crucial resources in fluctuating environments is particularly challenging for unicellular organisms. Under $K^+$-limiting conditions, induction of *kdpFABC* expression is controlled by the bifunctional sensor kinase KdpD via KdpE, which ultimately leads to production of the high-affinity KdpFABC transport system (Figures 1A and 1B). In this study, we show that KdpD is able to monitor concentrations of both extra- and intracellular $K^+$ and to regulate its dual function as an autokinase and a KdpE-specific phosphatase, according to the $K^+$ concentrations of the two $K^+$ pools (Figures 1C and 1D). The observed $K_{0.5}$ value for autokinase activity is in the range of environmental $K^+$ concentrations at which induction is observed in vivo, and amino acid replacements in the periplasmic loop of KdpD lead to loss of its sensitivity to external $K^+$. Furthermore, we demonstrated that the phosphatase activity is stimulated by intracellular $K^+$ via a sensor module located in the C-terminal cytoplasmic domain of KdpD (Figures 1, 2, and 4), although we cannot rule out additional regulation of phosphatase activity by extracellular $K^+$.

These results led us to formulate a dual-sensing, dual-regulation model for $K^+$-dependent KdpD signaling (Figure 5A), which reproduces the basic features of the system (Figures 5B and 5C). When the extracellular $K^+$ concentration is high (>5 mM), $K^+$ is recognized by the periplasmic loop and inhibits the autokinase activity. At the same time intracellular $K^+$ is sensed by the C-terminal cytoplasmic domain and stimulates the phosphatase activity. Consequently, KdpD acts as a phosphatase on KdpE-P,

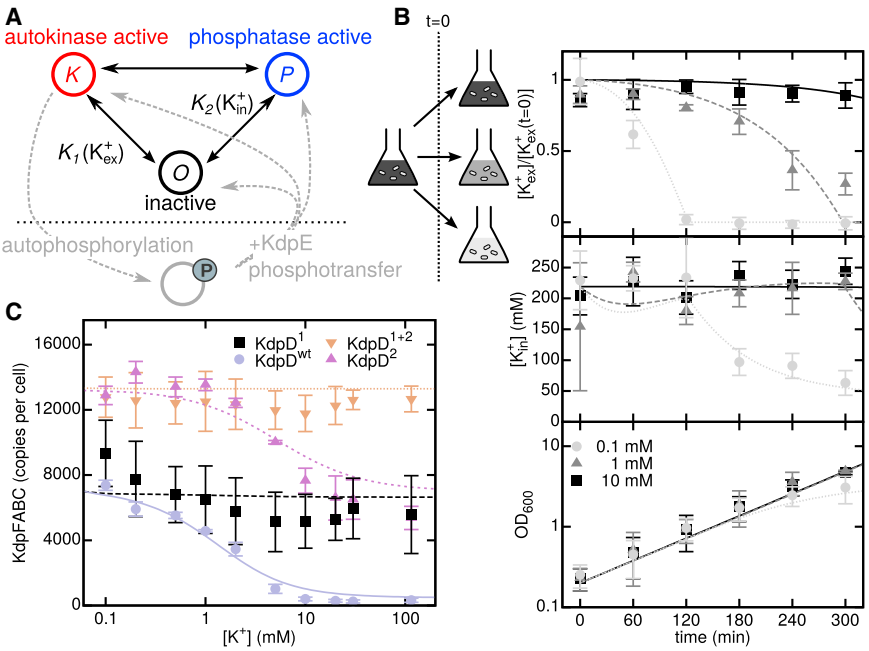


**Figure 5. Dynamics of Kdp Response In Vivo**

(A) Schematic of switching model of KdpD enzymatic activity. Autokinase and phosphatase activities are assumed to correspond to two distinct molecular conformations, *K* and *P*. A third inactive conformation, *O*, has no enzymatic activity. The equilibrium occupancy of each conformation is biased according to the extracellular and intracellular $K^+$ concentrations. Molecules in the *K* state can undergo autophosphorylation. Subsequently, phosphotransfer from phospho-KdpD to KdpE returns KdpD to each state according to their equilibrium occupancies.

(B) Dynamics of intracellular and extracellular $K^+$ concentrations for wild-type cells measured by atomic absorption spectroscopy and optical density at 600 nm. At time t = 0, cells were transferred from medium containing 10 mM $K^+$ to media with the indicated concentrations.

(C) KdpFABC levels were determined by quantitative western blot analysis, 120 min after transfer of cells to media with the indicated $K^+$ concentration. Data points are the mean ± SD of three biological replicates. Lines show results of the mathematical model.

and production of the high-affinity $K^+$ transporter is prevented. When environmental levels of $K^+$ fall below the threshold for autokinase activation, *kdpFABC* expression is initiated; however, as long as the intracellular $K^+$ concentration remains high, the KdpD phosphatase activity remains stimulated. Under these conditions, the intracellular response is attenuated for as long as the high intracellular $K^+$ concentration is sufficient for all cellular processes. The longer the cells are exposed to $K^+$ limitation or extreme $K^+$ limitation, the greater the drop in intracellular [$K^+$]. Eventually, the phosphatase activity is no longer stimulated and higher amounts of KdpE become phosphorylated, resulting in maximal production of KdpFABC.

Importantly, this dual-sensing, dual-regulation mechanism allows *E. coli* not only to respond to impending limitation by sensing the extracellular $K^+$ concentration but also to regulate the activation level in response to changing intracellular $K^+$ requirements. In particular, the demand for $K^+$ is determined by the cellular growth rate. In media that permit rapid growth, intracellular $K^+$ could become depleted even though it is abundant in the environment. Under these conditions, sensing of the intracellular $K^+$ level allows the cell to fine-tune its uptake rate to match the demand. We included this cellular scenario in our mathematical model, and we used simulations to compare the dual-sensing strategy to strategies with sensing of only one $K^+$ pool under variation of both environmental [$K^+$] and growth rate. We found that the dual-sensing strategy was better able to maintain intracellular [$K^+$] within the tolerable range, and, therefore, it was able to outcompete single-sensing strategies (Figure 6). The same regulatory dynamics can account for the induction of *kdpFABC* expression under other conditions that reduce the availability of free intracellular $K^+$, such as extracellular $Cs^+$ or low pH (Jung et al., 2001; Roe et al., 2000).

Dual sensing thus emerges as a highly optimized regulation strategy. The key advantage of this strategy is the ability to directly sense changes in both supply of and demand for the limiting resource. It is in fact analogous to strategies that are widely used in control engineering (Kilian, 2005). For example, temperature controllers often monitor both internal and external temperatures to control heating and cooling elements (Figure 7). In this case, dual sensing keeps room temperature constant in the face of unpredictable changes in the weather or when variables such as incident sunlight, room occupancy, or the opening of doors affect heat influx and leakage. However, whereas engineered control systems usually have separate sensors, controllers, and actuators, bacteria have found a remarkably compact and integrated solution in the case of the Kdp system, with KdpD providing the functions of the sensors, the controller, and, aided by KdpE, also the actuator (Figure 7). Combining dual sensing with sensor kinase bifunctionality increases the reliability of homeostasis by ensuring robustness to changes in the protein concentrations (Batchelor and Goulian, 2003; Shinar et al., 2007). Dual sensing could, in principle, also be implemented by integrating both signals to regulate only one enzymatic activity. However, the regulation of both activities, as we observed for KdpD, may provide additional advantages, such as increasing the dynamic range of signaling.

Our data do not identify the specific molecular transitions that determine the catalytic activities of KdpD, although we suggest that KdpD integrates distinct $K^+$ signals from at least two sensory domains. Structural data for conserved sensor kinase domains support the existence of distinct conformational states of bifunctional sensor kinases with autokinase or phosphatase activity (Marina et al., 2005; Ferris et al., 2012; Huynh and Stewart, 2011). Here we have used the simplest generalization of this conformational model to incorporate a third, enzymatically inactive state. However, the multidomain structure of KdpD potentially allows for a far larger number of conformations, as each domain may respond differently in the presence of distinct

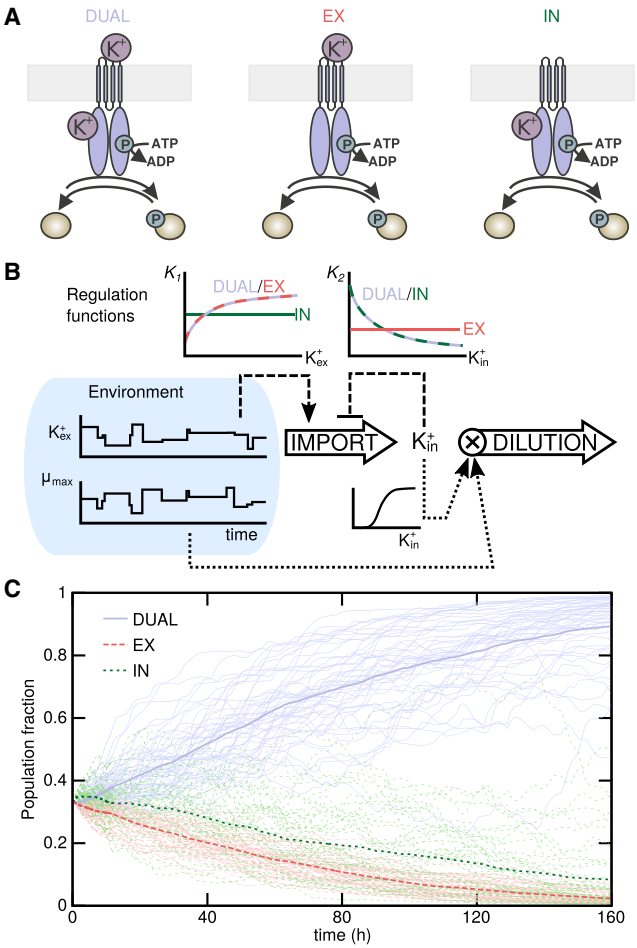


**Figure 6. Dual Sensing and Dual Regulation Provide Robust Control of Intracellular $K^+$**

(A) Illustrations show the three different regulation strategies. DUAL strategy, KdpD autokinase activity and phosphatase activity are regulated by both extracellular and intracellular $K^+$; EX strategy, both activities are regulated by extracellular $K^+$ independently of intracellular $K^+$; IN strategy, both activities are regulated by intracellular $K^+$ independently of extracellular $K^+$.

(B) Each strategy is characterized by the regulation functions that determine the enzymatic activities of KdpD as a function of the intra- and extracellular $K^+$. These control, via *kdpFABC* expression, the $K^+$ import rate. The rate of dilution of intracellular $K^+$ is the instantaneous growth rate, which is taken to be the product of the environmentally determined maximal growth rate, $\mu_{max}$, and a factor that depends on the intracellular $K^+$ level. Both $\mu_{max}$ and the environmental $K^+$ level are subject to fluctuations over time.

(C) Simulations of the outcome of competition among the three strategies. Starting from initially equal numbers of cells implementing each strategy, the plots depict the evolutionary trajectories of the subpopulations in environments in which both the extracellular $K^+$ supply and the maximal growth rate vary. Light lines show results for individual environmental realizations and thick lines show the mean over 50 realizations.

stimuli (Bhate et al., 2015). It therefore remains to be determined precisely how the dual $K^+$ stimuli are encoded in KdpD dynamics at a molecular scale.

The combination of extra- and intracellular sensing has been shown previously for $Mg^{2+}$ homeostasis in the pathogen *Salmonella enterica* serovar Typhimurium, albeit via a very different

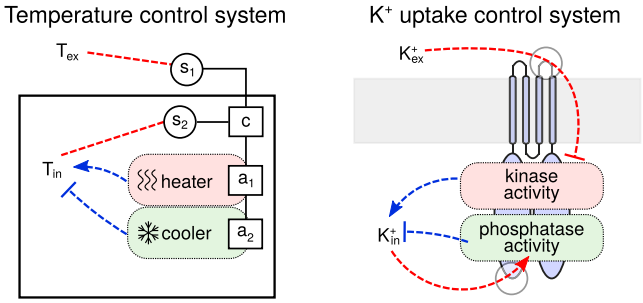


**Figure 7. Schematic Comparison of a Temperature Control System with KdpD**

A temperature controller (c) integrates measurements of the internal and external temperatures from individual sensors (s) into signals that regulate the actuators (a) of a heater and a cooler. KdpD is an all-in-one control system for $K^+$ uptake: it combines extracellular and intracellular sensing functions, which control its autokinase and phosphatase activities, respectively, as well as the actuators of the downstream pathway.

mechanism. The PhoP/PhoQ two-component system in *Salmonella* senses external $Mg^{2+}$ limitation to activate target gene expression (García Véscovi et al., 1996). In addition, transcription of the gene encoding the $Mg^{2+}$ transporter MgtA is influenced by intracellular $Mg^{2+}$. More precisely intracellular $Mg^{2+}$ binds to the *mgtA* 5′ UTR and terminates transcription via stem-loop formation (Cromie et al., 2006). The expression of *mgtA* is thus regulated by both the intra- and extracellular $Mg^{2+}$ concentrations. However, unlike the Kdp system, the two signals are not integrated at the level of the sensor kinase; instead, they act at different levels of the response pathway. Such different regulation mechanisms may have specific functional implications. For example, post-transcriptional regulation of transporters would allow for a faster response than can be achieved by transcriptional regulation, providing better adaptation to rapidly varying signals or limiting over-accumulation if resources suddenly become abundant after limitation. Indeed, it is likely that the Kdp system is not only controlled at the transcriptional level but also at the post-translational level by proteolysis (Heermann et al., 2014) and modulation of KdpFABC activity at high $K^+$ concentrations (Roe et al., 2000; Damnjanovic and Apell, 2014). For most signal transduction pathways, the precise signaling mechanism has remained elusive up to now, and it is conceivable that dual sensing by bifunctional receptors and other similarly elaborate mechanisms that integrate multiple signals is the rule rather than the exception.

## EXPERIMENTAL PROCEDURES

### Strains and Plasmids

All strains used in this study are listed in Table S1, oligonucleotides are listed in Table S2, and plasmids are listed in Table S3. For details of strain and plasmid construction, see the Supplemental Experimental Procedures.

### Phosphorylation and Dephosphorylation Assays

Membrane vesicles (see the Supplemental Experimental Procedures) containing ~0.2 mg/ml KdpD were incubated in phosphorylation buffer (50 mM Tris/HCl [pH 7.5], 10% glycerol [v/v], 0.5 M NaCl, 10 mM $MgCl_2$, and 2 mM DTT) at room temperature. Phosphorylation was initiated by the addition of 20 μM [$\gamma$-$^{32}$P]ATP (2.38 Ci/mmol). At different times, aliquots were removed and the

reaction was stopped by mixing with SDS sample buffer (Jung et al., 1997). After incubation for 3.5 min, purified KdpE (see the Supplemental Experimental Procedures) was added at a final concentration of 0.1 mg/ml to the KdpD-containing samples (resulting in a 1:2 dilution of KdpD, ATP, and $K^+$ concentration) and the incubation was continued. Additional aliquots were removed at different times and mixed with SDS sample buffer.

For dephosphorylation assays, 10His-KdpE-$^{32}$P was obtained as described (Jung and Altendorf, 1998). Dephosphorylation was initiated by the addition of membrane vesicles containing ~0.1 mg/ml of either KdpD or the purified C-terminal cytoplasmic domain KdpD/Δ2–498 (0.1 mg/ml), 20 mM $MgCl_2$ in the presence of 20 μM ATP-γ-S. To test for $K^+$-dependent dephosphorylation of KdpE, we added KCl at the indicated concentrations. In both assays the ionic strength was always kept constant at 0.5 M by supplementing with NaCl (Jung et al., 1997). At different times, aliquots were removed and the reaction was stopped by the addition of SDS sample buffer. All samples were immediately subjected to SDS-PAGE. Shortly before the end of electrophoresis, an [γ-$^{32}$P] ATP standard was loaded onto the gels. Gels were then dried and protein phosphorylation was detected by exposure of the gels to a Storage Phosphor Screen. Phosphorylated proteins were quantified by image analysis using Image Quant® software (GE Healthcare).

### Determination of Extracellular and Intracellular $K^+$ Concentrations

$K^+$ concentrations were determined by atomic absorption spectroscopy (Bossemeyer et al., 1989). Briefly, *E. coli* MG1655 (Table S1) was cultivated in minimal medium containing 10 mM $K^+$ (Epstein and Kim, 1971). Cells were collected by centrifugation and transferred into pre-warmed minimal medium containing 0.1, 1, and 10 mM $K^+$, respectively, and then incubated aerobically at 37°C for 2 hr. Aliquots (1 ml) were taken and centrifuged through 200 μl silicone oil (DC550) at 13,000 rpm for 2 min. The $K^+$ content of the cell pellets and the supernatants was then determined in an atomic absorption spectrometer (Varian AA240 Spectroscopy Instrument, Agilent Technologies). To determine the fraction of bound and freely diffusible $K^+$, 0.5-ml samples were collected and diluted in either 0.5 ml medium (total $K^+$) or 0.5 ml $_{dd}H_2O$ (bound $K^+$) (Bossemeyer et al., 1989). After centrifugation through silicone oil, the $K^+$ content of the cell pellets was determined by atomic absorption spectroscopy. The fraction of free $K^+$ is defined as the difference between the total $K^+$ content and the bound $K^+$ content. The intracellular concentrations were calculated by taking the number of cells per sample and the cytoplasmic volumes into account. Since it has been shown that cell volumes remain more or less constant during the experiments, an average value of $8.12 \times 10^{-16}$ l per cell was used in all calculations (Heermann et al., 2014).

### Determination of $P_{kdpFABC}$ Activity In Vivo

In vivo signal transduction was probed using *E. coli* strain HAK006 (Table S1) transformed with plasmids carrying *kdpD* or the corresponding variants (Table S3), as previously described (Epstein and Kim, 1971; Miller, 1992). Cells were grown in minimal medium containing different $K^+$ concentrations (Epstein and Kim, 1971) and harvested in the mid-exponential growth phase by centrifugation. β-Galactosidase activity was determined as described (Miller, 1992) and is given in Miller units. Strains carrying mutations *kdpD*$^1$, *kdpD*$^2$, and *kdpD*$^{1+2}$ (HS2, HS3, and HS4) (Table S1) were aerobically cultivated in minimal medium containing 5 mM $K^+$ at 37°C until $OD_{600}$ = 0.5, then they were shifted to minimal media containing different $K^+$ concentrations for 2 hr. After harvesting the cells, β-galactosidase activity was determined as described before (Miller, 1992).

### Determination of KdpFABC Production by Quantitative Western Blot Analysis

Levels of KdpFABC in *E. coli* strains were determined by quantitative western blot analysis. *E. coli* strains LF3, HS2, HS3, and HS4 (Table S1) were grown aerobically at 37°C to $OD_{600}$ = 0.5 in minimal media containing 10 mM $K^+$ (Epstein and Kim, 1971). Then the cells were shifted to minimal medium containing the indicated $K^+$ concentrations. After 2 hr the $OD_{600}$ was adjusted to 1 and aliquots of the cultures were collected by centrifugation. Cells were resuspended in SDS sample buffer and subjected to SDS-PAGE. Proteins were electroblotted onto a nitrocellulose membrane, and the blots were blocked with 5% (w/v) skim milk in buffer A (10 mM Tris/HCl [pH 7.4] and 0.15 M NaCl) for 1 hr. Anti-KdpB antibody (Heermann et al., 2009) was added at a final dilution of 1:10,000 and incubation was continued for 1 hr. After washing with buffer A, goat anti-rabbit IgG conjugated with alkaline phosphatase was added in a final dilution of 1:2,500, and incubation was continued for 1 hr. After washing thoroughly, blots were developed with substrate solution (50 mM $Na_2CO_3$ [pH 9.5], 0.01% [w/v] nitro-blue-tetrazolium, and 5 mg/ml 5-bromo-4-chloro-3-indolylphosphate). Blots were scanned at high resolution in 256 gray scales, imported as TIF files into ImageJ, and the amount of KdpB was quantified. For each biological replicate, we calibrated the mean of two technical replicates using previously measured molecule numbers (Heermann et al., 2014), by finding a linear scaling coefficient that minimized the total squared deviation for the wild-type strain at the $K^+$ concentrations for which measurements were available in both datasets. The scaling coefficient was applied to all samples on a given blot. Data represent the average values and SD of three independent biological replicates.

### Fitting of Autokinase and Phosphatase $K^+$ Dependency

To determine the initial reaction rate, samples were taken after 10 and 20 s for the autokinase activity and after 1 and 2 min to determine $K^+$-dependent dephosphorylation of KdpE. This slope was used as a measure of the enzymatic activity. To minimize day-to-day variability, the activities in each replicate dataset were scaled by a constant factor, chosen to minimize the mean-squared deviation among all datasets (three independent experiments for autokinase activity of wild-type KdpD; two independent experiments each for phosphatase activity of wild-type KdpD, KdpD/Δ2–498, and KdpD$^1$). The different datasets were then pooled, and non-linear least-squares fitting was performed on the pooled data via the Levenberg-Marquardt method. For autokinase activity of wild-type KdpD a model of the form $c_1 + c_2(K_{0.5}/([K^+] + K_{0.5}))$ was assumed. The resulting best-fit parameter values were $c_1$ = 0.18 a.u., $c_2$ = 0.82 a.u., and $K_{0.5}$ = 2.7 mM. A model of the form $c_1 + c_2([K^+]/([K^+] + K_{0.5}))$ was used for fitting of the phosphatase activity. Best-fit parameter values were as follows: for wild-type KdpD: $c_1$ = 0.25 a.u., $c_2$ = 0.75 a.u., and $K_{0.5}$ = 4.2 mM; for KdpD/Δ2–498: $c_1$ = 0.11 a.u., $c_2$ = 0.89 a.u., and $K_{0.5}$ = 34 mM; and for KdpD$^1$: $c_1$ = 0.33 a.u., $c_2$ = 0.67 a.u., and $K_{0.5}$ = 32 mM. Confidence regions were estimated by randomly sampling parameter space and including or excluding parameter sets according to F test relative to the best-fit parameters.

### Mathematical Model

Details of the mathematical model and simulations are provided in the Supplemental Experimental Procedures.

## SUPPLEMENTAL INFORMATION

Supplemental Information includes Supplemental Experimental Procedures, six figures, and three tables and can be found with this article online at http://dx.doi.org/10.1016/j.celrep.2016.05.081.

## AUTHOR CONTRIBUTIONS

H.S., R.H., and K.J. designed the experiments. H.S. performed the experiments. F.T. and U.G. developed the mathematical model and F.T. performed simulations. H.S., F.T., R.H., U.G., and K.J. wrote the manuscript.

## ACKNOWLEDGMENTS

This work was supported by the Deutsche Forschungsgemeinschaft: Center for integrated Protein Science Munich (CiPSM) (Exc114/2) and (JU270/15-1) (to K.J.) and Nanosystems Initiative Munich (NIM) (Exc4/2) and (GE1098/6-1) (to U.G.). F.T. was supported by a research fellowship of the Alexander von Humboldt Foundation. We thank Daniel Wilson (Gene Center Munich) and Erwin Frey (LMU Munich) for critically reading the manuscript and Andy Fohrmann for constructing plasmids encoding truncated KdpD variants (pPV5-3/ΔTM1-4, pBD/ΔTM1-4/10Gly, and pBD/ΔTM1-4/5[Gly,Ala]).

Received: February 29, 2016
Revised: April 15, 2016
Accepted: May 19, 2016
Published: June 16, 2016

## REFERENCES

Altendorf, K., Siebers, A., and Epstein, W. (1992). The KDP ATPase of *Escherichia coli*. Ann. N Y Acad. Sci. *671*, 228–243.

Batchelor, E., and Goulian, M. (2003). Robustness and the cycle of phosphorylation and dephosphorylation in a two-component regulatory system. Proc. Natl. Acad. Sci. USA *100*, 691–696.

Bhate, M.P., Molnar, K.S., Goulian, M., and DeGrado, W.F. (2015). Signal transduction in histidine kinases: insights from new structures. Structure *23*, 981–994.

Booth, I.R. (1985). Regulation of cytoplasmic pH in bacteria. Microbiol. Rev. *49*, 359–378.

Bossemeyer, D., Borchard, A., Dosch, D.C., Helmer, G.C., Epstein, W., Booth, I.R., and Bakker, E.P. (1989). $K^+$-transport protein TrkA of *Escherichia coli* is a peripheral membrane protein that requires other *trk* gene products for attachment to the cytoplasmic membrane. J. Biol. Chem. *264*, 16403–16410.

Brandon, L., Dorus, S., Epstein, W., Altendorf, K., and Jung, K. (2000). Modulation of KdpD phosphatase implicated in the physiological expression of the kdp ATPase of *Escherichia coli*. Mol. Microbiol. *38*, 1086–1092.

Buurman, E.T., McLaggan, D., Naprstek, J., and Epstein, W. (2004). Multiple paths for nonphysiological transport of $K^+$ in *Escherichia coli*. J. Bacteriol. *186*, 4238–4245.

Cann, M. (2007a). A subset of GAF domains are evolutionarily conserved sodium sensors. Mol. Microbiol. *64*, 461–472.

Cann, M.J. (2007b). Sodium regulation of GAF domain function. Biochem. Soc. Trans. *35*, 1032–1034.

Cromie, M.J., Shi, Y., Latifi, T., and Groisman, E.A. (2006). An RNA sensor for intracellular $Mg^{2+}$. Cell *125*, 71–84.

Damnjanovic, B., and Apell, H.-J. (2014). KdpFABC reconstituted in *Escherichia coli* lipid vesicles: substrate dependence of the transport rate. Biochemistry *53*, 5674–5682.

Epstein, W. (2003). The roles and regulation of potassium in bacteria. Prog. Nucleic Acid Res. Mol. Biol. *75*, 293–320.

Epstein, W., and Kim, B.S. (1971). Potassium transport loci in *Escherichia coli* K-12. J. Bacteriol. *108*, 639–644.

Ferris, H.U., Dunin-Horkawicz, S., Hornig, N., Hulko, M., Martin, J., Schultz, J.E., Zeth, K., Lupas, A.N., and Coles, M. (2012). Mechanism of regulation of receptor histidine kinases. Structure *20*, 56–66.

García Véscovi, E., Soncini, F.C., and Groisman, E.A. (1996). $Mg^{2+}$ as an extracellular signal: environmental regulation of *Salmonella* virulence. Cell *84*, 165–174.

Goujon, M., McWilliam, H., Li, W., Valentin, F., Squizzato, S., Paern, J., and Lopez, R. (2010). A new bioinformatics analysis tools framework at EMBL-EBI. Nucleic Acids Res. *38* (*Suppl*), W695–W699.

Heermann, R., and Jung, K. (2012). $K^+$ supply, osmotic stress and the KdpD/KdpE two-component system. In Two-component systems in bacteria, R. Gross and D. Beier, eds. (Norwich, UK: Caister Academic Press), pp. 181–198.

Heermann, R., Weber, A., Mayer, B., Ott, M., Hauser, E., Gabriel, G., Pirch, T., and Jung, K. (2009). The universal stress protein UspC scaffolds the KdpD/KdpE signaling cascade of *Escherichia coli* under salt stress. J. Mol. Biol. *386*, 134–148.

Heermann, R., Zigann, K., Gayer, S., Rodriguez-Fernandez, M., Banga, J.R., Kremling, A., and Jung, K. (2014). Dynamics of an interactive network composed of a bacterial two-component system, a transporter and $K^+$ as mediator. PLoS ONE *9*, e89671.

Heikaus, C.C., Pandit, J., and Klevit, R.E. (2009). Cyclic nucleotide binding GAF domains from phosphodiesterases: structural and mechanistic insights. Structure *17*, 1551–1557.

Huynh, T.N., and Stewart, V. (2011). Negative control in two-component signal transduction by transmitter phosphatase activity. Mol. Microbiol. *82*, 275–286.

Jung, K., and Altendorf, K. (1998). Individual substitutions of clustered arginine residues of the sensor kinase KdpD of *Escherichia coli* modulate the ratio of kinase to phosphatase activity. J. Biol. Chem. *273*, 26415–26420.

Jung, K., Tjaden, B., and Altendorf, K. (1997). Purification, reconstitution, and characterization of KdpD, the turgor sensor of *Escherichia coli*. J. Biol. Chem. *272*, 10847–10852.

Jung, K., Krabusch, M., and Altendorf, K. (2001). $Cs^+$ induces the *kdp* operon of *Escherichia coli* by lowering the intracellular $K^+$ concentration. J. Bacteriol. *183*, 3800–3803.

Kilian, C.T. (2005). Modern Control Technology (Delmar Thomson Learning).

Laermann, V., Ćudić, E., Kipschull, K., Zimmann, P., and Altendorf, K. (2013). The sensor kinase KdpD of *Escherichia coli* senses external $K^+$. Mol. Microbiol. *88*, 1194–1204.

Lüttmann, D., Heermann, R., Zimmer, B., Hillmann, A., Rampp, I.S., Jung, K., and Görke, B. (2009). Stimulation of the potassium sensor KdpD kinase activity by interaction with the phosphotransferase protein IIA(Ntr) in *Escherichia coli*. Mol. Microbiol. *72*, 978–994.

Marina, A., Waldburger, C.D., and Hendrickson, W.A. (2005). Structure of the entire cytoplasmic portion of a sensor histidine-kinase protein. EMBO J. *24*, 4247–4259.

Mével-Ninio, M., and Yamamoto, T. (1974). Conversion of active transport vesicles of *Escherichia coli* into oxidative phosphorylation vesicles. Biochim. Biophys. Acta *357*, 63–66.

Miller, J.H. (1992). A short course in bacterial genetics: a laboratory manual and handbook for *Escherichia coli* and related bacteria (Plainview, N.Y.: Cold Spring Harbor Laboratory Press).

Nissen, P., Hansen, J., Ban, N., Moore, P.B., and Steitz, T.A. (2000). The structural basis of ribosome activity in peptide bond synthesis. Science *289*, 920–930.

Roe, A.J., McLaggan, D., O'Byrne, C.P., and Booth, I.R. (2000). Rapid inactivation of the *Escherichia coli* Kdp $K^+$ uptake system by high potassium concentrations. Mol. Microbiol. *35*, 1235–1243.

Rothenbücher, M.C., Facey, S.J., Kiefer, D., Kossmann, M., and Kuhn, A. (2006). The cytoplasmic C-terminal domain of the *Escherichia coli* KdpD protein functions as a $K^+$ sensor. J. Bacteriol. *188*, 1950–1958.

Shinar, G., Milo, R., Martínez, M.R., and Alon, U. (2007). Input output robustness in simple bacterial signaling systems. Proc. Natl. Acad. Sci. USA *104*, 19931–19935.

Willett, J.W., and Kirby, J.R. (2012). Genetic and biochemical dissection of a HisKA domain identifies residues required exclusively for kinase and phosphatase activities. PLoS Genet. *8*, e1003084.

Zeng, Y., Han, X., and Gross, R.W. (1998). Phospholipid subclass specific alterations in the passive ion permeability of membrane bilayers: separation of enthalpic and entropic contributions to transbilayer ion flux. Biochemistry *37*, 2346–2355.